Available online at www.sciencedirect.com
SCIENCE DIRECT®
Remote Sensing of Environment 89 (2004) 176–188
Remote Sensing of Environment
www.elsevier.com/locate/rse

Retrieval of the canopy leaf area index in the BOREAS flux tower sites using linear spectral mixture analysis

Baoxin Hu[a,b,*], John R. Miller[a], Jing M. Chen[c], Allan Hollinger[b]

[a] Department of Earth and Atmospheric Science, York University, Toronto, Canada
[b] Canadian Space Agency, Saint-Hubert, Quebec, Canada
[c] Department of Geography, University of Toronto, Toronto, Canada

Received 26 February 2001; received in revised form 4 June 2001; accepted 15 June 2002

Abstract

This paper reports on the use of linear spectral mixture analysis for the retrieval of canopy leaf area index (LAI) in three flux tower sites in the Boreal Ecosystem-Atmosphere Study (BOREAS) southern study area: Old Black Spruce, Old Jack Pine, and Young Jack Pine (SOBS, SOJP, and SYJP). The data used were obtained by the Compact Airborne Spectrographic Imager (CASI) with a spatial resolution of 2 m in the winter of 1994. The convex geometry method was used to select the endmembers: sunlit crown, sunlit snow, and shadow. Along transects for these flux tower sites, the fraction of sunlit snow was found to have a higher correlation with the field-measured canopy LAI than the fraction of sunlit crown or the fraction of shadow. An empirical equation was obtained to describe the relation between canopy LAI and the fraction of sunlit snow. There is a strong correlation between the estimated LAI and the field-measured LAI along transects (with R^2 values of 0.54, 0.71, and 0.60 obtained for the SOBS, SYJP, and SOJP sites, respectively). The estimated LAI for the whole tower site is consistent with that obtained by the inversion of a canopy model in our previous study where values of 0.94, 0.92, and 0.63 were obtained for R^2 for the SOBS, SYJP and SOJP sites, respectively.

The CASI 2-m summer data over the SOBS site was also employed to investigate the possibility of deriving canopy LAI from the summer data using linear mixture analysis. At a spatial resolution of 10 m, the correlation between the field-measured LAI and the estimated LAI along transects is small at R^2 less than 0.3, while R^2 increases to 0.6 at a spatial resolution of 30 m. The difficulty in canopy LAI retrieval from the summer data at a spatial resolution of 10 m is likely due to the variation of the understory reflectance across the scene, although spatial misregistration of the CASI data used may also be a possible contributing factor.

Keywords: Leaf area index; BOREAS; Linear spectral mixture analysis

1. Introduction

The canopy leaf area index (LAI) is a very important parameter in modelling ecosystem processes and the exchanges of energy, momentum, and mass between the biosphere and the lower atmosphere (e.g., Dickinson, 1995; Hall, Townshend, & Engman, 1995; Hall, Shimabukuro, & Huemmrich, 1995). Retrieval of the canopy LAI for different biomes from remote sensing data is, therefore, an active research area (e.g., Hall, Townshend et al., 1995; Hall, Shimabukuro et al., 1995). The openness of the overstory and the spatial and temporal variations of the understory vegetation in the boreal forests pose special challenges to the retrieval of canopy leaf area index (LAI) from remotely sensed data. For example, the results presented in Leochel et al. (1997) show that the correlation between the canopy LAI and vegetation indices for the boreal forest stands is, in general, small with R^2 less than 0.3. Chen and Cihlar (1996) estimated the canopy LAI from the normalized difference vegetation index (NDVI) derived from TM images over the Boreal Ecosystem-Atmosphere Study (BOREAS) flux tower sites. The correlation between the retrieved LAI and the field-measured LAI was small, with R^2 of 0.5 in the late spring and 0.42 in midsummer examples of their results. These research reports suggest that the confounding effects of understory vegetation are important to the interpretation of reflectance

* Corresponding author. Petrie Science Building, Room 255, York University, 4700 Keele Street, Toronto, ON, Canada M3J 1P3. Tel.: +1-416-736-2100; fax: +1-416-736-5516.
E-mail address: baoxin@terra.phys.yorku.ca (B. Hu).

0034-4257/$ - see front matter © 2003 Elsevier Inc. All rights reserved.
doi:10.1016/j.rse.2002.06.003

of sparse canopies typical in the boreal forest. As a result, the utility of vegetation indices for retrieving the canopy LAI for boreal forest canopies may be very limited, in contrast to satisfactory results obtained from the application of spectral vegetation indices to agricultural canopies (e.g., Sellers, 1985, 1987).

An alternate approach to retrieval of the canopy LAI is to invert a canopy reflectance model (Goel, 1988). Rosema et al. (1992) introduced the forest-light interaction model (FLIM) to derive LAI and canopy coverage (Rosema et al., 1992) from TM data over the Kootwijk Forest in the Netherlands. Hu, Inannen, and Miller (2000) modified the FLIM and produced canopy LAI and canopy closure maps for the BOREAS flux tower sites using the Compact Airborne Spectrographic Imager (CASI) winter data. A strong correlation has been found between the retrieved canopy LAI and the field-measured LAI along the transects (Chen, Rich, Gower, Norman, & Plummer, 1997) using such model-based methods, for example, with R^2 values between 0.51 and 0.86 (Hu et al., 2000). In addition, recent enhancement of our use of the FLIM has been reported by Fernandes, Hu, Miller, and Rubinstein (2000) for boreal canopies with significant clumping, such as for black spruce, through the addition of ray tracing features in a new algorithm called FLIM-CLUS.

Another approach to the retrieval of open canopy parameters is linear spectral analysis. Linear spectral mixture analysis of multispectral and hyperspectral remote sensing data sets has been widely used in geology applications (e.g., Mustard & Sunshine, 1999). For vegetation applications, Hall, Townshend et al. (1995) and Hall, Shimabukuro et al. (1995) employed linear spectral mixture analysis and a geometric optical model to infer the biomass density from the shadow fraction. Other biophysical parameters, such as canopy LAI, can then be derived based on their relationship with the biomass density (Hall, Townshend et al., 1995; Hall, Shimabukuro et al., 1995). In this study, the application of linear spectral mixture analysis in the retrieval of the canopy LAI for the boreal forest canopies is investigated using the CASI winter data containing a relatively uniform and spectrally featureless snow background. The potential to retrieve the canopy LAI using the CASI summer data is also investigated. The results obtained by linear spectral mixture analysis are compared with those obtained previously by canopy model inversion (Hu et al., 2000).

2. CASI data and study sites

The CASI airborne imaging spectrometer sensor was deployed extensively at BOREAS for acquisition of multispectral and hyperspectral imagery in the visible and near-infrared spectral bands (Miller et al., 1995). During the BOREAS field campaigns in the winter of 1994 and in the summer of 1996, several CASI images with the spatial resolution of 2 m were obtained over flux tower sites in the BOREAS southern study area and northern study area. In this study, the CASI images over Young Jack Pine (SYJP), Old Jack Pine (SOJP), and Old Black Spruce (SOBS) in the southern study area were employed. The BOREAS southern study regions are located in Saskatchewan, Canada (http://boreas.gsfc.nasa.gov). The flux tower sites lie in areas with relatively homogeneous vegetation cover.

The CASI image data used have been calibrated to radiance (Gray et al., 1997), atmospherically corrected (O'Neill et al., 1997) to above-canopy reflectance, and geo-referenced (Cosandier, Ivanco, & Mah, 1992). The CASI winter data have seven spectral bands as follows: 449.61–521.63, 520.41–566.05, 564.83–601.69, 620.11–651.73, 650.53–682.21, 776.53–821.21, and 840.03–890.43 nm. The solar zenith angle was 75°, 69°, and 76° for the SOBS, SYJP, and SOBS sites, respectively. Zenith nominal nadir view was assumed for all of the three sites. For these sites, a tree crown has a size similar to the spatial resolution of the CASI imagery (2 m). A pixel would therefore typically contain only part of a tree crown. To make canopy LAI meaningful on a pixel basis, we spatially degraded the CASI imagery. For canopy models using geometric optical theory, a pixel is assumed to contain a tree crown and its shadow (Li & Strahler, 1992). Considering potential use of a canopy model in this study, the original 2-m CASI winter images were spatially degraded to 30 m to increase the probability that a tree crown and its shadow occur in the same pixel.

2.1. Linear spectral mixture analysis

The linear spectral mixture model describes the surface reflectance spectrum as a linear combination of a finite number of spectra corresponding to the pure components, called endmembers. With an ideal choice of the endmembers, the coefficients representing the component fractional areas in the linear model are nonnegative and sum to 1. When photons interact with multiple components within the field of view, such as the multiple scattering between the vegetation canopy and soil, the mixture has the potential of becoming nonlinear (Johnson, Smith, Taylor-George, & Adams, 1983). So far, there has been abundant research that reports that the linear mixture model has wide utility in remote sensing applications (e.g., Mustard & Sunshine, 1999; Hall, Townshend et al., 1995; Hall, Shimabukuro et al., 1995).

The most difficult and crucial step in linear mixture analysis is the selection of spectral endmembers. Four approaches are commonly used. (1) Obtain the endmember spectra from a spectrum library. The successful use of this approach is strongly dependent on the calibration of the image data used. It is further complicated when differences between inherent and apparent reflectance of surface features are considered as a result of the canopy 3-D

structure. (2) Derive the endmember spectra from the pure pixels of the image itself. This approach can only be used in cases where there are some pure pixels in the image data examined. (3) Automatically obtain endmember spectra using factor analysis. For this approach, abstract matrices corresponding to endmember spectra and the fraction of the endmembers are first calculated based on the pure mathematics. Then, a transformation matrix is built, or an iterative approach is used to transform the abstract matrices to ones with physical meanings (i.e., the real endmember spectra and their fractions) (Malinowski & Howery, 1980). Many approaches have been developed to obtain the transform matrix. These methods are based on some intuitive criteria of the factor space, such as simple structure and hypothetical structure (Rummel, 1970). An interactive approach, target transform, has been successfully applied in chemistry applications such as in resolving highly overlapping chromatographic peaks (e.g., Gamperline, 1986). In this approach, test data are needed. (4) Automatically construct endmember spectra using convex geometry. Boardman (1992) successfully applied this approach to AVIRIS (Airborne Visible/Infrared Imaging Spectrometer, Vane et al., 1993) data for both vegetation and geological applications. In this study, the convex geometry method was used to estimate the endmember spectra.

Convex geometry deals with the geometry of convex sets (Valentine, 1964). A convex set in n-dimensional space is defined as a set of points that are linear combinations of a finite number of points, where the weights are all positive and sum to unity. This is the same definition as the linear mixture model. To clearly describe this approach, it is useful to discuss the following two notions in convex geometry: convex hull and simplex (Brody, 2001). Assume S is a set of points in an n-dimensional space. By definition, the convex hull of S is the smallest convex set that contains the set S. The simplex is a convex set with $n+1$ vertices. It gives a unique decomposition for all points in the set S. Craig (1990) proposed the "smallest" simplex containing the data as the "best" simplex. That is, the "best simplex" has the smallest "volume." The vertices of the "best" simplex are considered as the endmembers of the set S. For the analysis of image data for the SOBS, SYJP, and SOJP sites, we are only interested in pixels corresponding to the jack pine or black spruce canopies. Some pixels, such as those with white and bright red tone in the colour composite image shown in the left panels of Fig. 1, do not contain the canopy of interest for these sites. For simplicity, the pixels with the canopy of interest for the flux tower sites (BS in the SOBS site, JP in the SYJP site and in the SOJP site) are denoted as target pixels, whereas others pixels are referred to as nontarget pixels. To avoid the effects of the nontarget pixels on the selection of endmembers, the whole image was first segmented into target pixels and nontarget pixels for each site using an image cluster algorithm called NGCLUS2 in PCI (PCI, 1999). The near-infrared band (band 6, 776.53–821.21 nm), the red band (band 5, 650.53–682.21 nm), and the green band (band 3, 564.83–601.69 nm) were used in the segmentation process. The results are presented in middle panels of Fig. 1, where the target pixels have a white tone, and nontarget pixels (snow or snow with other nontarget canopies) are displayed as grey. Referring to the left panels of Fig. 1, one can note that most of the nontarget pixels are around the access trail to the tower and in open areas. Some pixels with a bright red tone were also classified into nontarget class. It is likely that wintering deciduous shrubs with a bright snow background contribute to these bright pixels. The target and nontarget pixels can also be clearly distinguished in the two-dimensional space defined by the first two principal components of these CASI images, as shown in the left panels of Fig. 2. For the SOBS and SOJP sites, the target pixels cluster closely together, and the pixels out of the cluster are nontarget pixels. For the SYJP site, the pixels of the whole image evidently form two clusters. The one on the left contains target canopy. The other includes nontarget pixels. It is worth mentioning that due to limits on the accuracy of the image segmentation, some forested pixels with a very low percentage of targeted canopy (such as OBS for the SOBS site, YJP for the SYJP site, and OJP for the SOJP site) may be classified into nontarget pixels. In future studies, an advanced image segmentation approach should be employed to improve the segmentation accuracy.

After image segmentation, principal component analysis (PCA) for the seven spectral bands of the CASI winter images was performed for the target pixels in each tower site. The first two principal components explain 99.8%, 99.9%, and 99.7% of the variance of the target pixels in the seven spectral bands for the SOBS, SYJP, and SOJP sites, respectively. Therefore, only the first two principal components were employed. As a result, all of the target pixels for each flux tower site can be described as points in the two-dimensional space defined by the first two principal components and are shown in the middle panels of Fig. 2. According to the theory of convex geometry (Brody, 2001), the "smallest" simplex with three vertices can be found to decompose all of the points in the two-dimensional space. The three vertices of the 'smallest" simplex are the endmembers. Physically, the landscape with single-species forest with snow background, as is the case in this study, may be modeled in spectral mixture analysis with three endmembers such as sunlit crown, sunlit snow, and shadow.

The software Qhull (http://www.geom.umn.edu/locate/qhull) was used to find the convex hull of the data cloud shown in the middle panels of Fig. 2. The endmembers were then determined by constructing the "smallest" simplex (a triangle with minimum area for this study) that contains the convex hull. For the CASI data used here, the first principal component corresponds to brightness infor-

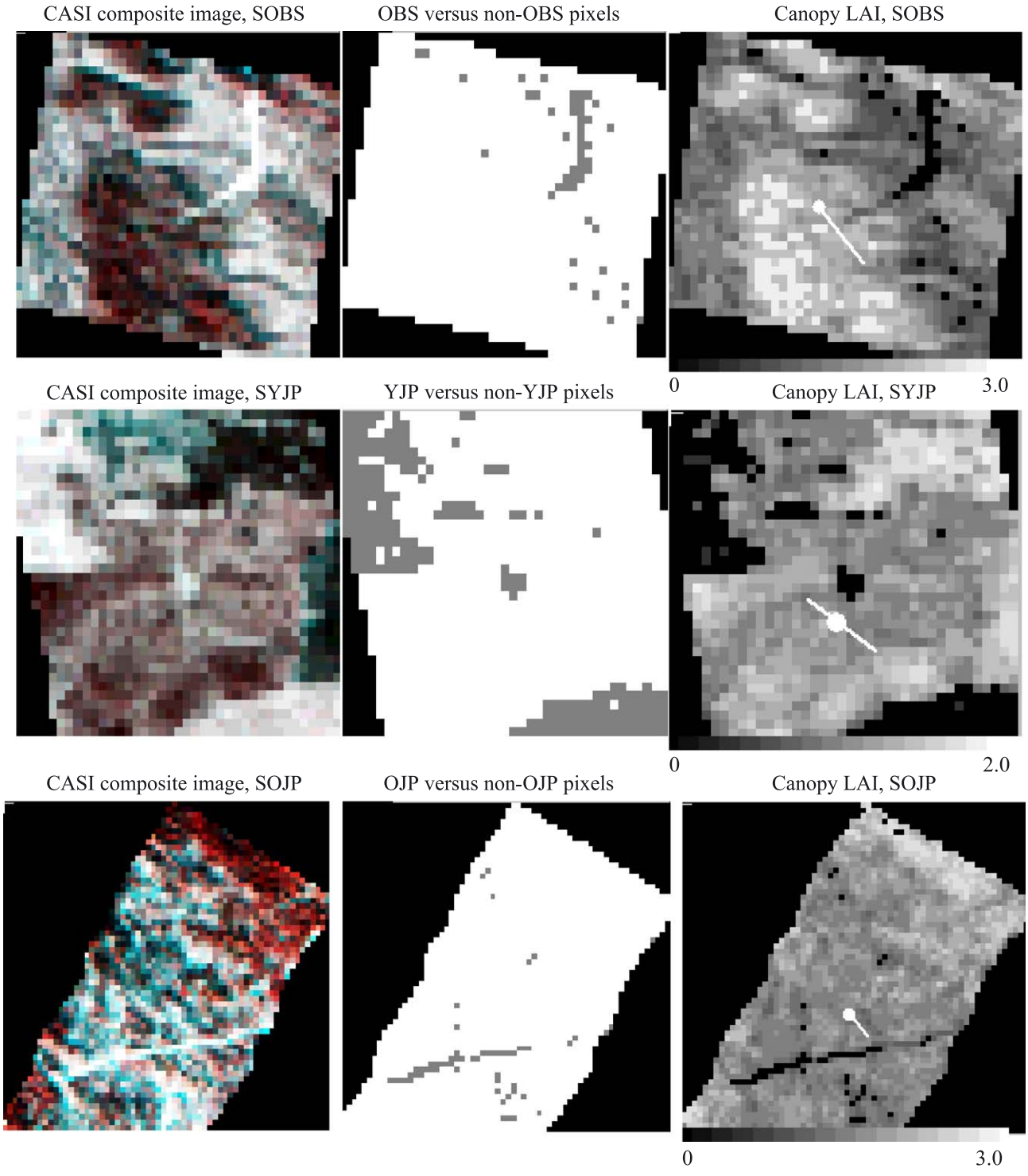

Fig. 1. The CASI colour composite images and the resulting images for the SOBS, SYJP and SOJP sites. The spatial resolution is 30 m. The colour composite images (left panels) are printed with the near-infrared band (band 6, 776.53–821.21 nm) as red, red band (band 5, 650.53–682.21 nm) as green, and the green band (band 3, 564.83–601.69 nm) as blue. The target pixels obtained after image segmentation are shown as a bright tone in the middle panel. The right panels present the canopy LAI. The tower position and transect B (Chen et al., 1997) is marked in the right panels for these three tower sites.

mation, in that it is the weighted sum of reflectance in the seven spectral bands. The second principal component is the difference in reflectance between the visible bands and the near-infrared bands, and therefore, this principal component is associated with the greenness of the scene. As a result, the sunlit crown should have a low value in the first principal component and a large negative value in the second principal plane. The sunlit snow should have a very large value in the first principal component and a low absolute value in the second principal component. Shad-

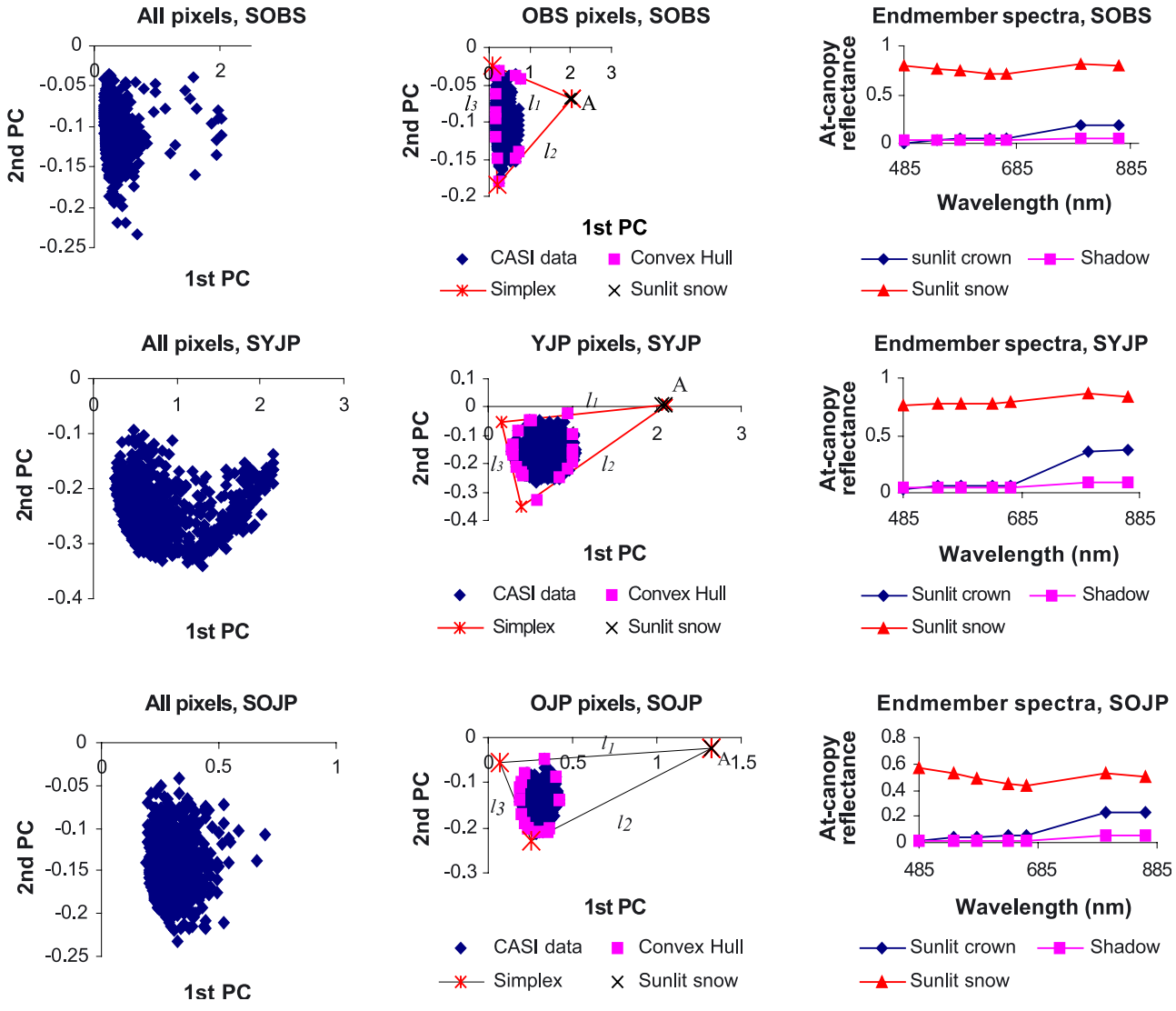

Fig. 2. The endmembers and their spectra for the SOBS, SYJP and SOJP sites. Left panels: all pixels in the 2-D space defined by the first two principal components. Middle panels: the target pixels, the convex hull, and the simplex that contains these pixels. Right panels: the endmember spectra.

ows have low energy and thus should have a very low value in the first principal component and a low absolute value in the second principal component. As seen in Fig. 1, there are open areas or access trails in these sites. Accordingly, a couple of sunlit snow pixels were selected in the open areas or access trails after verification by checking spectra of the pixels and are displayed in Fig. 2. The central point of these sunlit snow pixels was selected as one endmember or one vertex of the simplex, denoted as "A". l_1 and l_2 are two tangent lines from A to the convex hull, and two sides of the simplex are on l_1 and l_2. To find the third side, a line was drawn, denoted as l_3, passing through two points of the convex hull. These two points were selected so that l_1, l_2, and l_3 can enclose the data cloud, and the simplex formed by these three lines has a minimum area among all possible triangles enclosing the data cloud. The intersected points between l_1, l_2, and l_3 are the three vertices of the simplex and also the three endmembers. We then performed the inverse PCA to the selected endmembers to get the endmember spectra. As a result of this somewhat subjective procedure, the endmembers and their spectra that emerged for the SOBS, SYJP, and SOJP canopies are presented in Fig. 2. As expected, the sunlit crown has the typical vegetation spectra, the sunlit snow has a high reflectance, and shadow has a low reflectance. For the SOJP site, Soffer, Miller, Wanner, and Strahler (1995) reported the reflectance spectra of sunlit crown, sunlit snow, shadowed crown, and shadowed snow measured from above the SOJP canopy on February 7, 1994 under conditions similar to those encountered during the CASI winter data acquisition. The spectra of sunlit crown and sunlit snow obtained in this study are similar to those obtained by Soffer et al. (1995) within the standard errors reported. It may not be clear why the reflectance of sunlit snow is observed to be quite low for the SOJP site. This may be attributed to the facts that the reflectance in

both the CASI data and in Soffer et al. (1995) was calculated with respect to the top of canopy irradiance, and also that the transmittance of solar radiation through the SOJP canopy is small. A methodology to automatically construct the ''smallest'' simplex from features within an image is a priority of our future research. It is hoped that this will reduce the uncertainties in determining the vertices and will improve the efficiency of information retrieval.

After the endmember spectra are determined, the following constrained linear equations need to be solved to obtain the fractions of these three endmembers:

$$R(\lambda) = f_c R_c(\lambda) + f_g R_g(\lambda) + f_s R_s(\lambda), \quad (1)$$

where,

$$0 \le f_c \le 1,\ 0 \le f_g \le 1,\ 0 \le f_s \le 1,$$

and

$$f_c + f_g + f_s = 1,$$

where $R(\lambda)$ is the reflectance of a pixel and is the function of the wavelength λ; $R_c(\lambda)$, $R_g(\lambda)$, and $R_s(\lambda)$ are the spectral reflectances of the three endmembers: sunlit crown, sunlit snow, and shadow, respectively; and the coefficients, f_c, f_g, and f_s are the areal fractions of sunlit crown, sunlit snow and shadow, respectively. For each target pixel in the CASI images for the SOBS, SYJP, SOJP sites, the above equations were solved to estimate the areal fractions of the endmembers.

2.2. Derivation of the canopy LAI from the fractions of the endmembers

The retrieval of canopy LAI, not the fractions of the endmembers, is the objective of our linear spectral analysis. Accordingly, our investigation began with an examination of the correlation between the fraction of the endmembers and the field-measured canopy LAI.

Chen et al. (1997) presented the field-measured canopy LAI for the BOREAS flux tower sites. The canopy LAI values at the flux tower sites were measured every 10 m along parallel transects A, B, and C during the BOREAS intensive field campaign in 1993. The location of transect B is marked in Fig. 1 and transects A and C are parallel to transect B with a separation distance of 10 m to each side (see Chen et al., 1997, for details). The field-measured LAI values (for simplicity, only the effective LAI is used in this analysis and is referred to as LAI) were averaged for use in this study. First, the field-measured LAI values along each transect were subjected to a sliding average of three measurements (separated by 20 m), and then the resulting values were averaged between the three parallel transects. The field-measured LAI versus the fractions of sunlit snow, sunlit crown, and shadow along transect are shown in Fig. 3 for the SOBS, SYJP, and SOJP sites. Overall, the fraction of sunlit snow has a stronger correlation with the field-measured canopy LAI than the fraction of shadow or the fraction of sunlit crown.

Hall, Townshend et al. (1995), Hall, Shimabukuro et al. (1995) Hall, Peddle, and LeDrew (1996), and Peddle, Hall, and LeDrew (1999) concluded that the shadow fraction is a better predictor of biophysical variables than the fractions of sunlit crown and sunlit understory. These conclusions were based on biomass, LAI, and aboveground net primary productivity (NPP) data for the black spruce stands in the Superior National Forest, Minnesota, USA, during the summers of 1983 and 1984 for solar zenith angles between 30° and 60°. In their studies, the reflectance of sunlit crown was estimated using a cylindrical crown canopy model; from their results, they concluded that the fraction of sunlit background was the best predictor for the canopy LAI (Hall, Townshend et al., 1995; Hall, Shimabukuro et al., 1995; Peddle et al., 1999). Using a conical tree canopy model, the fraction of sunlit background was shown to be better for predicting biomass, LAI, and NPP than the fraction of shadow for a large solar zenith angle such as 60° (Hall et al., 1996; Peddle et al., 1999). When a spheroid model was used, the shadow fraction was the best for predicting biomass, LAI, and NPP for solar zenith angles between 30° and 60°, especially for 45°. These results taken together suggest that either the shadow fraction or the fraction of sunlit background can be used to predict the canopy biophysical parameters. In this study, the reflectance of each of the three endmembers, sunlit crown, sunlit snow (background), and shadow, was derived directly from the data rather than from model estimates. Our results for solar zenith angles greater than 70°, shown in Fig. 3, demonstrate that the fraction of sunlit snow is better for predicting canopy LAI, when compared to the prediction from the fraction of sunlit crown and shadow.

The background snow can be seen in both the illumination direction and the observation direction through the gaps between crowns and the gaps within the crowns. According to Rosema et al. (1992), the fraction of the sunlit snow is composed of four components. The first component is the area under crowns in both illumination and observation directions (denoted as F_{cd}). It is dependent on the transmittance through tree crowns in the illumination direction (T_s) and in the observation direction (T_v). The second component is the area open in the illumination direction and under crowns in the observation direction (F_{cs}) and depends on the transmittance through tree crowns in the observation direction (T_v). The third component is the area under crowns in the illumination direction and open to the observation direction (F_{od}) and is dependent upon the transmittance through tree crowns

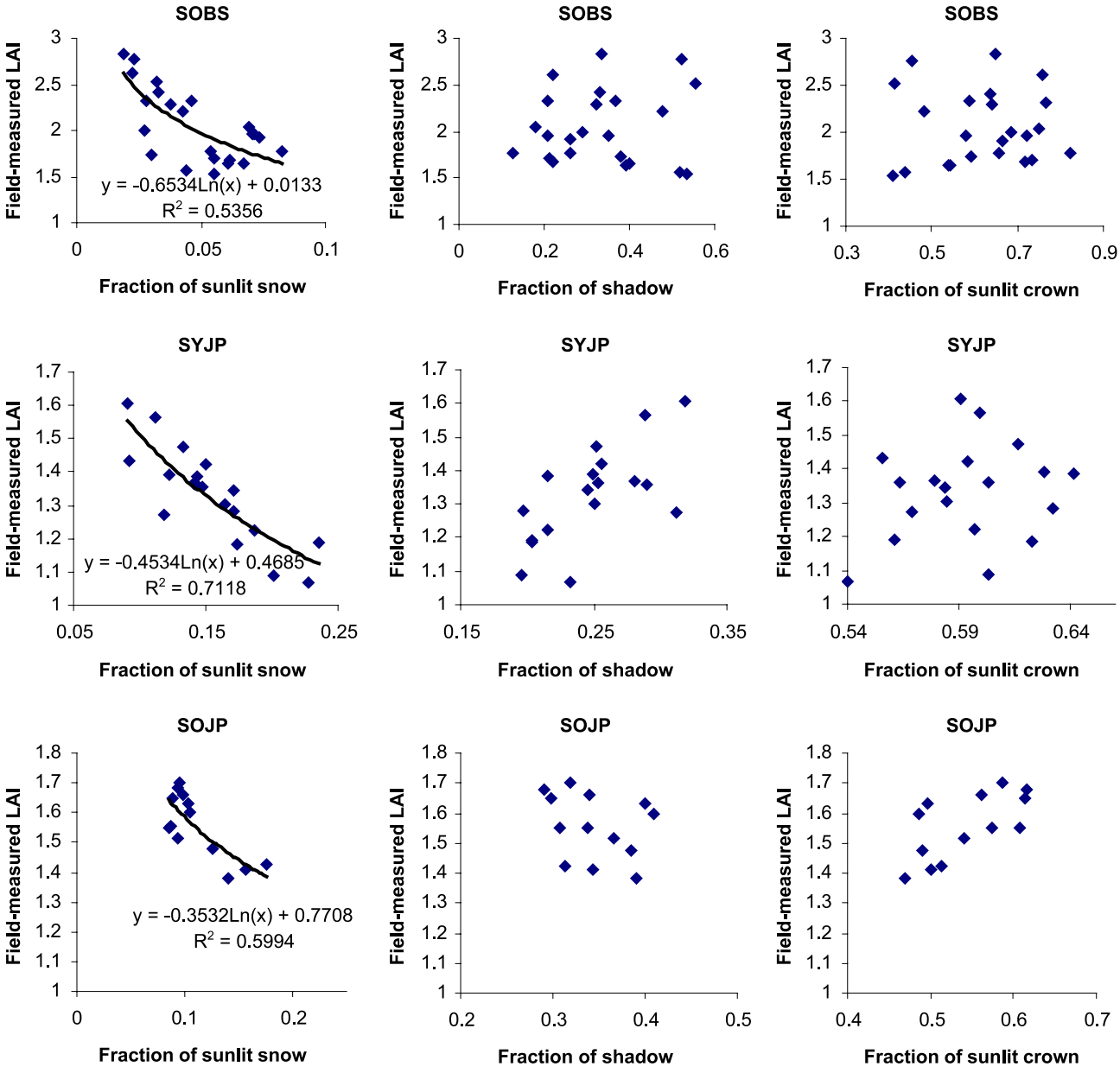

Fig. 3. The correlation of the fractions of the sunlit snow, shadow, and sunlit crown with the field-measured canopy LAI along the transect (Chen et al., 1997) for the SOBS, SYJP, and SOJP sites.

in the illumination direction (T_s). The last component is the open spaces in both illumination and observation directions (F_{os}). Therefore, the fraction of sunlit background G is

$$G = F_{cd}T_sT_v + F_{cs}T_v + F_{od}T_s + F_{os}. \quad (2)$$

The first three terms in Eq. (2) are related to the within-crown gap probability in the illumination direction and/or observation direction. The last term is controlled by the between-crown gap probability in both the illumination and the observation directions and is also the fraction of sunlit snow under the assumption of a completely opaque crown. The fraction of sunlit snow is a function of canopy LAI through its dependence upon crown coverage and crown LAI.

Since canopy LAI is included in radiative transfer models of the canopy as an exponential term, a logarithmic function was used to fit the field-measured LAI versus the fraction of sunlit snow. The R^2 correlation between the field-measured LAI and the fraction of sunlit snow is 0.54, 0.71, and 0.60 for the SOBS, SYJP, and SOJP sites, respectively. The coefficients (slope and offset) obtained above vary for each canopy. To understand the physical meaning of the slope and offset, a more detailed examination of the calculation of the fraction of sunlit snow is provided below.

For the imaging geometry away from the hotspot, as the case in this study, F_{cd}, F_{cs}, F_{od}, and F_{os} can be calculated by the following equations (Rosema et al., 1992).

$$F_{cd} = C_v C_s, \tag{3}$$

$$F_{cs} = C_v(1 - C_s), \tag{4}$$

$$F_{od} = (1 - C_v)C_s, \tag{5}$$

$$F_{os} = (1 - C_v)(1 - C_s), \tag{6}$$

where C_v and C_s are the crown coverage in the direction of observation and illumination, respectively. The equations to calculate T_s and T_v are as follows (Hu et al., 2000):

$$T_v = \exp\left(-G(\theta_v)L_e \frac{C_{nadir}}{C_v \cos(\theta_v)}\right), \tag{7}$$

$$T_s = \exp\left(-G(\theta_s)L_e \frac{C_{nadir}}{C_s \cos(\theta_s)}\right). \tag{8}$$

In Eqs. (6) and (7), C_{nadir} is the crown coverage at nadir; θ_v and θ_s are the view zenith angle and solar zenith angle, respectively; and L_e is the average effective leaf area index of crowns defined as the ratio of the effective canopy leaf area index and the crown coverage at nadir. In this paper and in Hu et al. (2000), the effective leaf area index (LAI) of the canopy is simply denoted L_e(canopy). $G(\theta_v)$ and $G(\theta_s)$ are the fraction of total foliage area that is perpendicular to the view zenith angle θ_v and the solar zenith angle θ_s, respectively. As mentioned above, the solar zenith angle was 75°, 69°, and 76° for the SOBS, SYJP, and SOBS sites, respectively, and the view zenith angle was assumed to be zero for all three sites. Due to the large solar zenith angle and large ellipticity of the tree crown (the ratio of the vertical radius to the horizontal radius), especially for the black spruce canopy, C_s is much greater than C_{nadir} (or C_v), and thus, T_s is much smaller than T_v. We therefore approximated Eq. (2) as follows:

$$G = F_{cs}T_v + F_{os} = C_v(1 - C_s)\exp(-G(\theta_v)L_e) + (1 - C_v)(1 - C_s), \tag{9}$$

and

$$L_e = -\frac{1}{G(\theta_v)}[\ln(G - (1 - C_v)(1 - C_s)) - \ln(C_v(1 - C_s))], \tag{10}$$

$$L_e(\text{canopy}) = -\frac{C_v}{G(\theta_v)}[\ln(G - (1 - C_v)(1 - C_s)) - \ln(C_v(1 - C_s))] = -\frac{C_v}{G(\theta_v)} \times \left[\ln G - \ln\frac{G}{G - (1 - C_v)(1 - C_s)} - \ln(C_v(1 - C_s))\right]. \tag{11}$$

Although the canopy LAI is not exactly a simple logarithmic function of G as expressed in Eq. (11), some insight is provided about the slope and offset obtained above. The slope is always negative. The offset can be positive or negative, depending mainly upon the contribution of the between-crown gap probability on the fraction of sunlit snow. For the SOBS sites, the ellipticity of the Old Black Spruce crown is much larger than that of the jack pine crown in the SYJP and SOJP sites, and thus, between-crown gap probability in the SOBS site tends to be smaller than that in the SOJP and SYJP sites. The offset is therefore expected to be a greater value for both the SYJP and the SOJP sites than the SOBS site.

Based on the empirical equations obtained by curve fitting the field-measured LAI to the sunlit snow fraction (shown in the plots of Fig. 3), the canopy LAI was estimated for the SOBS, SYJP, and SOJP sites. The resulting LAI images are shown in the right panels of

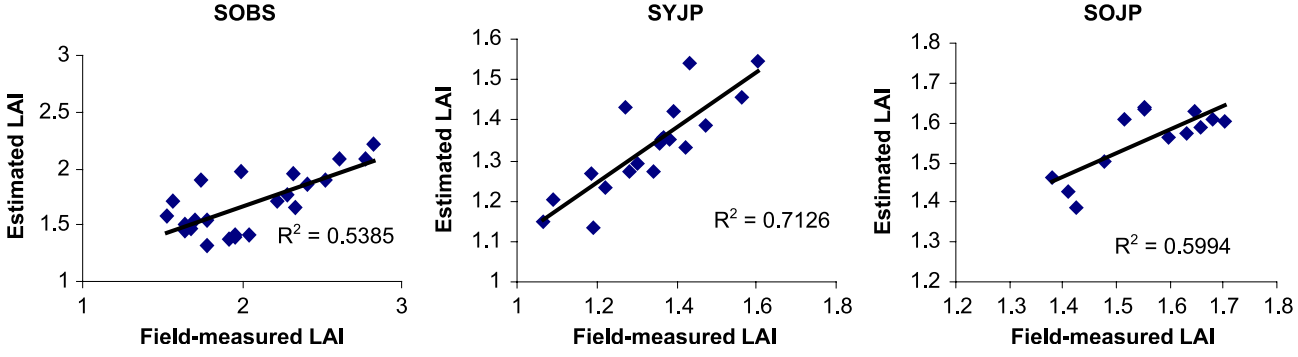

Fig. 4. The correlation between the field-measured LAI and the LAI derived from linear spectral mixture analysis along the transect for the SOBS, SYJP, and SOJP sites.

Fig. 1. As the images show, the canopy LAI images follow the spatial patterns exhibited by the colour composite images. For example, the dense canopy area (dark red in the colour composite image) has high canopy LAI (bright in the LAI image). The estimated canopy LAI along the transect was then compared with the field-measured LAI (Chen et al., 1997), and the results are shown in Fig. 4. The R^2 correlation between the estimated LAI and the field-measured LAI is 0.54, 0.71, and 0.60 for the SOBS, SYJP, and SOJP sites, respectively. The relative root mean square error (rmse, relative to the field-measured LAI) between them is 0.27, 0.057, and 0.042 for the SOBS, SYJP, and SOJP sites, respectively. It is clear that although the correlation between the estimated LAI and the field-measured LAI is strong for all three sites, the relative rmse between them is quite large for the SOBS site. The Old Black Spruce crown clusters tightly, and the ellipticity of the tree crown is very large. These features of the SOBS canopy may raise problems in the application of the linear spectral analysis due to the linear assumption, an issue that has been addressed in the FLIM-CLUS algorithm presented by Fernandes et al (2000).

As mentioned earlier, we produced the LAI images for the same flux tower sites in an earlier study using a canopy reflectance model, FLIM (Hu et al., 2000). Comparisons between the results obtained in this study and those presented in Hu et al. (2000) are presented in Fig. 5, which shows that an R^2 correlation of the canopy LAI of the target pixels is 0.94, 0.92, and 0.63 for the SOBS, SYJP, and SOJP sites, respectively. The comparison indicates good consistency of the canopy LAI obtained using the two approaches. Presumably, this is because the FLIM model expresses the reflectance of the scene viewed by the sensor as the weighted sum of the ground reflectance and the reflectance of a homogeneous and infinitely deep forest canopy. That is, the FLIM model is a linear mixture model as well. Since the FLIM model is a physical model, the results may also imply that the derived empirical equation based on the data along transects can be applied across the entire area around the tower for the investigated tower sites.

3. Derivation of the canopy LAI from CASI summer images using the linear mixture analysis

In our previous study (Hu et al., 2000), we performed a sensitivity analysis based on the FLIM (Hu et al., 2000), which indicated that the at-canopy reflectance is more sensitive to the understory reflectance than to the canopy LAI at the CASI viewing geometry (nadir observation). This result challenges the viability of LAI retrievals using the canopy reflectance model with the summer image data where the understory reflectance exhibits evident spatial variations in the boreal forest sites investigated. The CASI summer image over the SOBS site was used to investigate the effect of the understory reflectance on the retrieval of the canopy LAI using the FLIM. The R^2 correlation between the field-measured LAI and the retrieved LAI, with the assumption that each understory vegetation had a uniform reflectance for each understory vegetation (feather moss or sphagnum), was as low as 0.27. The R^2 correlation increased to 0.78 when the understory reflectance was allowed to vary within the range of the mean value plus or minus its standard deviation obtained by field measurement (Miller et al., 1997).

In this study, we investigated the possibility to use linear mixture analysis described above to derive the canopy LAI from a CASI summer image for the SOBS site. The CASI summer image over the SOBS site was obtained on July 30, 1996 with a spatial resolution of 2 m. It had 16 spectral bands ranging from 412.5 to 935.3 nm. The solar zenith angle was 45°, and the view zenith angle was $\pm 7°$ from nadir and was treated as nadir. The CASI 2-m summer images over the SOBS site were spatially degraded into images with a spatial resolution of 10 m to be used to derive the canopy LAI. Because there are much higher sun elevation angles in the summer (typically >60°) than in the winter (<20°), 10-m pixels in the summer data contain both sunlit crowns and their shadows cast on the ground.

Following the procedure described above, the spatially degraded CASI summer image was first segmented into OBS pixels and non-OBS pixels using band 11 (774.6 nm), band 7 (677.4 nm), and band 5 (645.2 nm). Then, principal

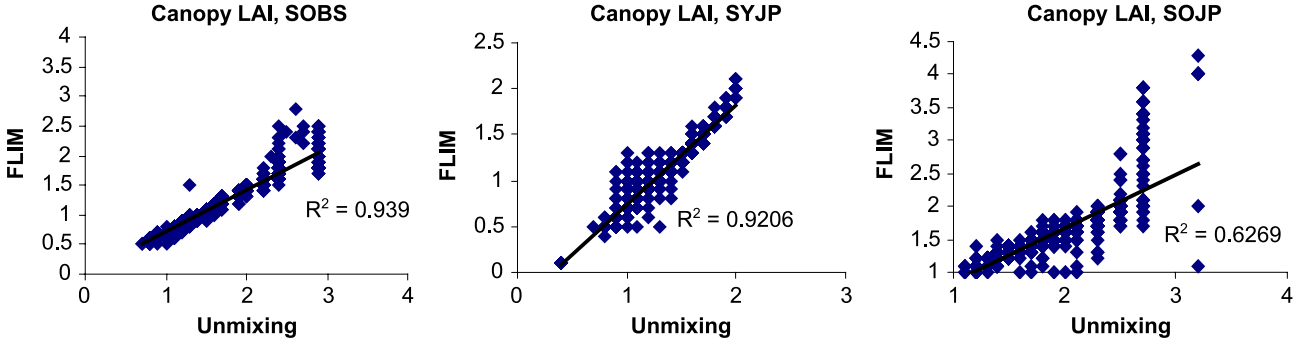

Fig. 5. The correlation between the canopy LAI obtained by the linear mixture analysis and that obtained by the inversion of the FLIM (Hu et al., 2000).

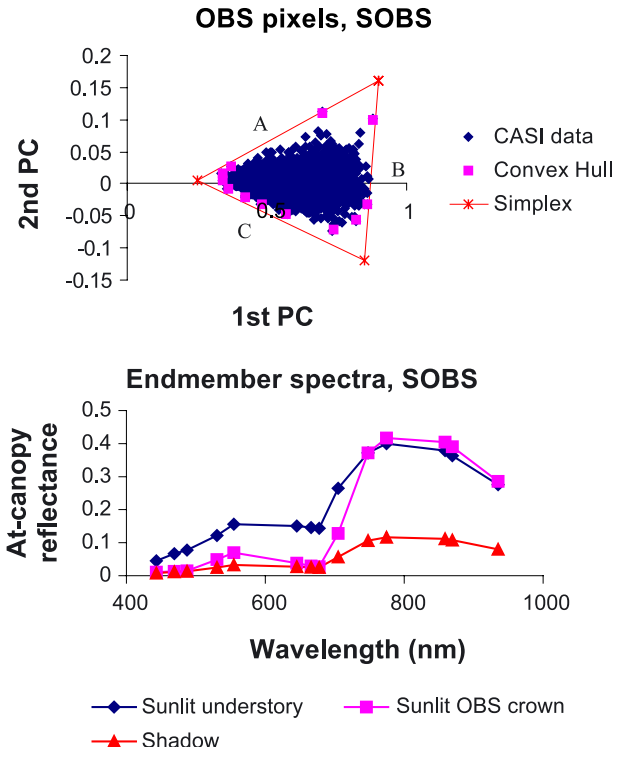

Fig. 6. The endmembers and their spectra derived from the CASI summer image over the SOBS site.

component analysis (PCA) was performed to the OBS pixels based on bands 2–15 (from 442.9 to 869.3 nm). The first two principal components were found to contain 98.8 % of the information. Accordingly, the first two principal components were used to estimate the endmembers and their spectra. The upper panel in Fig. 6 shows the OBS pixels in the 2-D space composed by the first two principal components. Like the CASI winter data, in the CASI summer data, the first principal component is associated with brightness of the scene, and the second one presents its greenness. Using the convex geometry method employed for the winter data, we obtained the three endmembers, and their spectra are shown in the bottom panel of Fig. 6. The sunlit understory pixels could not be found in the summer data. To find the endmembers, three lines were drawn through two points of the convex hull on sides A, B, and C, respectively. These points were selected to minimize the area of the triangle formed by these three lines among all possible triangles enclosing the data cloud. The intersected points between these three lines are the endmembers. As expected, the reflectance of the sunlit understory has a higher reflectance in the visible band and lower reflectance in the near-infrared band than the sunlit OBS crown, consistent with measurements of Miller et al. (1997). Solving Eq. (1) based on the estimated endmember spectra, we obtained the fractions of sunlit understory, shadow, and sunlit OBS crown.

The relation between the sunlit understory and field-measured LAI along the transects (Chen et al, 1997) were also investigated. The R^2 correlation between the sunlit understory and field-measured LAI is 0.27 for transect A, 0.23 for transect B, and 0.019 for transect C. The results indicate that it is problematic to retrieve canopy LAI from the CASI summer data using the linear mixture analysis at a spatial resolution of 10 m. Two possible factors explain this observation. First, the understory reflectance varies across the whole scene, violating the assumption of constant endmember spectra in linear mixture analysis. Second, there are inaccuracies in the spatial co-registration of the CASI imagery and the field transects, and the assumption that a 10-m resolution is consistent with LAI field data collected with the LAI-2000 is not assured.

Considering that the variation of both the understory and overstory reflectance tends to decrease when the spatial resolution decreases, there is a potential to retrieve the

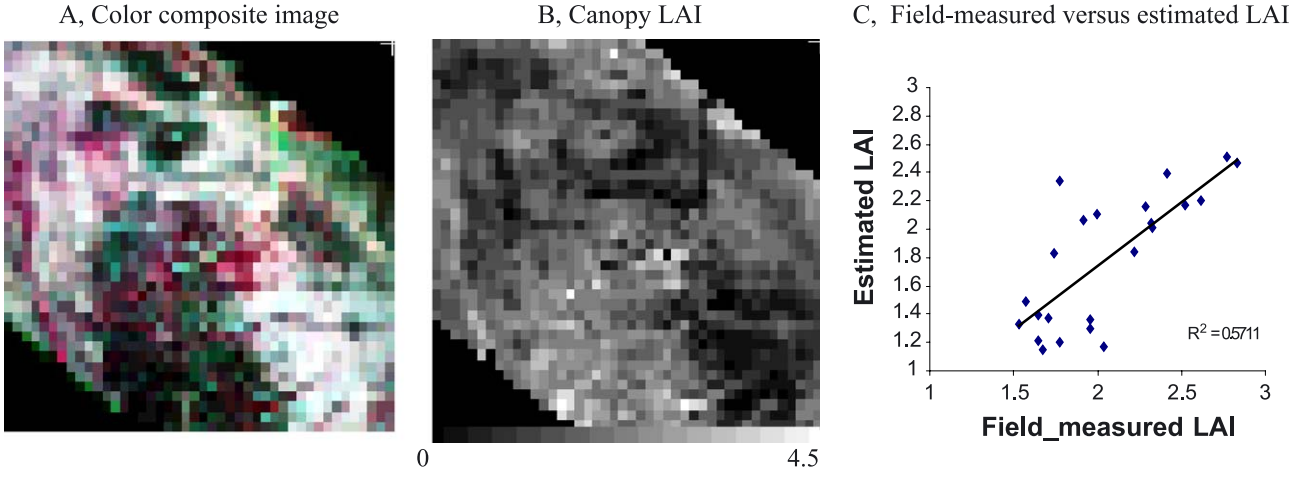

Fig. 7. Panel A: The CASI summer colour composite image with band 11 (774.6 nm) displayed as red, band 7 (677.4 nm) as green, and band 5 (645.2 nm) as blue. Panel B: The canopy LAI estimated by the empirical equation obtained by the field-measured LAI and the fraction of sunlit snow from linear mixture analysis. Panel C: The correlation between the estimated LAI and the field-measured LAI along the transect. The spatial resolution of the images is 30 m.

canopy LAI from the summer image at a coarser spatial resolution, such as 30 m. To explore this idea, we repeated the above analysis for the summer data at a spatial resolution of 30 m. This was accomplished by spatially degrading the 2-m summer data to 30 m. The field-measured LAI was also averaged for our analysis at the spatial resolution of 30 m, which reduces the variation of the canopy LAI, caused by measurement errors. The R^2 correlation between the fraction of sunlit understory and the field-measured LAI increased to 0.60.

Based on the empirical equation obtained by the curve fitting (shown in the plots in Fig. 6), we estimated the canopy LAI for this site. The resulting LAI image is shown in Panel B of Fig. 7. As the image shows, the canopy LAI image follows the spatial patterns exhibited by the colour composite image shown in Panel A of Fig. 7. The estimated canopy LAI along the transect was compared with the field-measured LAI (Chen et al, 1997), and the result is shown in Panel C of Fig. 7. The R^2 correlation between the estimated LAI and the field-measured LAI is 0.57. This result is similar to that obtained from CASI winter data.

4. Discussion and conclusions

In this study, linear mixture analysis was applied to CASI winter imagery to derive the fraction of sunlit crown, sunlit snow, and shadow for the SOBS, SYJP, and SOJP flux tower sites. It was used to obtain the canopy LAI for these flux tower sites as well. The methodology that was proposed in this study could be used to analyse airborne and spaceborne multispectral imagery. Segmentation of the whole image into target and nontarget pixels at each flux tower site can facilitate the selection of the endmembers, because it limits the number of the endmembers. Segmentation also makes the spectra of the endmembers distinct from each other. The segmentation approach can be extended to the processing of remotely sensed imagery covering several overstory canopies. For such a case, these different overstory canopies are first identified, and then linear mixture analysis is performed for each overstory canopy.

The convex geometry method was used to select endmembers in this study. This approach is effective and easy to understand, and neither pure pixels nor a spectrum library is needed. However, at present, this approach is suitable only for cases with a small number of endmembers (Craig, 1990). This limitation can be overcome by segmenting the image into different areas.

The fraction of sunlit snow obtained by the linear mixture analysis was demonstrated to have a higher correlation with the field-measured canopy LAI along the transects for the SOBS, SYJP, and SOJP sites (Chen et al., 1997) than the fraction of sunlit crown or the fraction of shadow. This conclusion is different from that derived by Hall, Townshend et al. (1995), Hall, Shimabukuro et al. (1995), Hall et al. (1996), and Peddle et al. (1999). In those studies, the reflectance of the sunlit crown was estimated by geometric optical canopy reflectance models, and the fraction of shadow was selected as the best predictor of biophysical parameters (such as biomass, LAI, and NPP). However, we can also find some cases in their data where the fraction of sunlit background is a better choice particularly for large solar zenith angle. In our study, the reflectance of each of the three endmembers was derived from the data themselves. Considering the large solar zenith angles used in our work, our results are consistent with those obtained by Hall, Townshend et al. (1995), Hall, Shimabukuro et al. (1995), and Hall et al. (1996). However, our results also demonstrate that for the SOBS site, the fraction of shadow cannot be used to estimate the canopy LAI in the winter scene.

An empirical equation was obtained to calculate the canopy LAI from the fraction of sunlit snow by fitting a logarithmic function to the data (field-measured LAI vs. fraction of sunlit snow) along the transect. The R^2 correlation between the field-measured LAI and the estimated LAI is 0.54, 0.71, and 0.60 along the transects for the SOBS, SYJP, and SOJP sites, respectively. The relative rmse (relative to the field-measured LAI) between them is 0.27, 0.057, and 0.042 for the SOBS, SYJP, and SOJP site, respectively. The large rmse for the SOBS site may be because the at-canopy reflectance is not a linear sum of the reflectance of sunlit crown, sunlit snow, and shadow. Since the CASI image covers a relatively homogeneous area for each flux tower site investigated, we used the empirical equation obtained from the transect, describing the relation between the canopy LAI and the fraction of sunlit snow, to obtain the canopy LAI for other pixels. The canopy LAI for the whole area around each tower is shown to have a good consistency with that obtained by the inversion of the FLIM (Hu et al., 2000) with a R^2 of 0.94, 0.92, and 0.63 for the SOBS, SYJP, and SOJP sites, respectively. Although the results are encouraging, the spectral mixture analysis to LAI retrieval is site dependent.

An alternative approach to obtaining the canopy LAI from the fractions of sunlit snow, sunlit crown, and shadow is to use a canopy model. Pure radiative transfer models, such as SAIL model (Verhoef, 1984), have been developed to describe the reflectance properties of agriculture canopies. Pure geometric optical models, such as the Li and Strahler (1992) model, assume that the tree crown is a solid object. Most hybrid radiative transfer and geometric optical models, such as the GORT model (Li, Strahler, & Woodcock, 1995), are not linear. As mentioned earlier, the FLIM model treats the reflectance of the scene viewed by the sensor as the weighted sum of the ground reflectance and the reflectance of a homogeneous and infinitely deep forest canopy. In this study, we investigated the use of the FLIM in deriving the canopy LAI from the fractions of the three endmembers. The correlation between the derived LAI and the field-measured LAI along the transect is strong with a R^2 correlation of 0.54, 0.70, and 0.60 for the SOBS, SYJP, and SOJP sites, respectively. Since the FLIM considers neither

the contribution of shadow nor the mutual shadowing of the tree crowns to the at-canopy reflectance, the FLIM may not be an optimum choice for this investigation. A better model should be developed in future studies.

The CASI summer data over the SOBS site was also employed to investigate the possibility of deriving the canopy LAI from summer data using linear mixture analysis. At a spatial resolution of 10 m, the correlation between the field-measured LAI and the estimated LAI is small with the R^2 correlation less than 0.3. The R^2 correlation increases to 0.6 at a spatial resolution of 30 m. These results suggest that it may not be possible to derive the canopy LAI from the summer data at a spatial resolution of 10 m. This is mainly due to the variation of the understory reflectance across the scene or due to spatial misregistration of CASI data due to limitation in the sensor navigational data as deployed in the research project.

Overall, the canopy LAI derived from CASI winter imagery and summer imagery with a spatial resolution of 30 m using linear spectral mixture analysis has a better agreement with the field-measured LAI than that obtained using vegetation indices using TM imagery for the same area (Chen & Cihlar, 1996). The derived canopy LAI for the SOBS, SYJP, and SOJP sites can be exploited by experts in forest ecosystem functioning.

Acknowledgements

We gratefully acknowledge the Canadian Space Agency for support to participate in the BOREAS Follow-On Program. The CASI processed data available for this study are due to extraordinary efforts of scientists at the Centre for Research in Earth & Space Technology, Jim Freemantle and Lawrence Gray, as well as subsequent support from Geomatics for Informed Decisions (GEOIDE), one of the Canadian Networks of Centres of Excellence.

References

Boardman, J. W. (1992), Automating spectral unmixing of AVIRIS data using Convex geometry. In R. O. Green (Ed.), *Summaries of the 4th Airborne Geoscience Conference* (pp. 243–270). JPL Publication 90-54, Pasadena, CA: Jet Propulsion Laboratory.

Brody, J. (2001). *Endmember extraction of hyperspetral data using convex simplex hull*. Report to Canadian Space Agency, St-Hubert, Quebec, Canada.

Chen, J., & Cihlar, J. (1996). Retrieval of leaf area index of boreal conifer forests using Landsat TM images. *Remote Sensing of Environment*, *55*, 153–162.

Chen, J., Rich, P. M., Gower, S. T., Norman, J. M., & Plummer, S. (1997). Leaf area index of boreal forests: Theory, techniques, and measurements. *Journal of Geophysical Research*, *102*, 29429–29443.

Cosandier, D., Ivanco, T., & Mah, S. (1992). The geocorrection and integration of the global positioning system with the Compact Airborne Spectrographic Imager. *Proceedings of the 15th Canadian Symposium on Remote Sensing* (pp. 385–390). Ottawa, Ontario: Canadian Remote Sensing Society, Canadian Aeronautics and Space Insitute.

Craig, M. (1990). Unsupervised unmixing of remotely sensed images. *Proceedings of the Fifth Australian Remote Sensing Conference, Perth, Australia* (pp. 324–330).

Dickinson, R. E. (1995). Land processes in climate models. *Remote Sensing of Environment*, *51*, 27–38.

Fernandes, R. A., Hu, B., Miller, J. R., & Rubinstein, I. G. (2000). A multi-scale approach to mapping effective leaf area index in Boreal Picea mariana stands using high-resolution CASI imagery. *International Journal of Remote Sensing*, *23,* 2547–2568.

Gamperline, P. J. (1986). Target transformation factor analysis with linear inequality constraints applied to spectroscopic-chromatographic data. *Analytical Chemistry*, *58*, 2656–2663.

Goel, N. S. (1988). Models of vegetation canopy reflectance and their use in estimation of biophysical parameters from reflectance data. *Remote Sensing Reviews*, *4*, 1–212.

Gray, L., Freemantle, J., Shepherd, P., Miller, J., Harron, J., & Hersom, C. (1997). Characterization and calibration of the CASI airborne imaging spectrometer for BOREAS. *Canadian Journal of Remote Sensing*, *23*, 188–195.

Hall, F. G., Shimabukuro, Y. E., & Huemmrich, K. F. (1995). Remote sensing of forest biophysical structure using mixture decomposition and geometric reflectance model. *Ecolgical Applications*, *5*, 993–1013.

Hall, F. G., Townshend, J. R., & Engman, E. T. (1995). Status of remote sensing algorithms for estimation of land surface state paremeters. *Remote Sensing of Environment*, *51*, 138–156.

Hall, F. G., Peddle, D. R., & LeDrew, E. F. (1996). Remote sensing of biophysical variables in boreal forest stands of Picca Mariana. *International Journal of Remote Sensing*, *17*, 3077–3081.

Hu, B., Inannen, K., & Miller, J. R. (2000). Retrieval of Leaf Area Index and canopy closure from CASI data over the BOREAS flux tower sites. *Remote Sensing of Environment*, *74*, 255–274.

Johnson, P. E., Smith, M. O., Taylor-George, S., & Adams, J. B. (1983). A semi-empirical method for analysis of the reflectance spectra of binary mineral mixtures. *Journal of Geophysical Research*, *88*, 3557–3561.

Leochel, S. E., Walthall, C. L., Brown de Colstoun, E., Chen, J., Markham, B. L., & Miller, J. (1997). Variability of boreal forest reflectances as measured from a helicopter platform. *Journal of Geophysical Research*, *102*, 29495–29503.

Li, X., & Strahler, A. H. (1992). Geometric-optical bi-directional reflectance modelling of the discrete crown vegetation canopy: Effect of crown shape and mutual shadowing. *IEEE Transactions on Geoscience and Remote Sensing*, *30*, 276–291.

Li, X., Strahler, A. H., & Woodcock, C. E. (1995). A hybrid geometric optical-radiative transfer approach for modelling albedo and directional reflectance of discontinuous canopies. *IEEE Transactions on Geoscience and Remote Sensing*, *33*, 466–480.

Malinowski, E. R., & Howery, D. G. (1980). *Factor analysis in chemistry.* New York: Wiley.

Miller, J. R., Freemantle, J., Shepherd, P., et al. (1995). Development of CASI to meet the needs of BOREAS science. *Proceedings of the 17th Canadian Symposium on Remote Sensing, Saskatoon, Saskatchewan, 13–15 June* (pp. 169–175). Ottawa, Canada: The Canadian Aeronautics and Space Institute.

Miller, J. R., White, H. P., Chen, J. M., McDermid, G., Pedde, D., Fournier, R., Shepherd, P., Rubenstein, I., Freemantle, J., Scoffer, R., & Ledrew, E. (1997). Seasonal change in understory reflectance of boreal forests and influence on canopy vegetation indices. *Journal of Geophysical Research*, *102*, 29475–29482.

Mustard, J. F., & Sunshine, J. M. (1999). Spectral analysis for earth science investigation. In A. N. Rencz (Ed.), *Remote sensing for the earth sciences*. New York: Wiley.

O'Neill, N. T., Zagolski, F., Bergeron, M., Royer, A., Miller, J., & Freemantle, J. (1997). Atmospheric correction of CASI images acquired over the BOREAS southern study area. *Canadian Journal of Remote Sensing*, *23*, 143–162.

PCI Geomatics (1999). *Using PCI Software*. 50 West Wilmot street, Richmond Hill, Ontario, Canada, L4B 1M5.

Peddle, D. R., Hall, F. G., & LeDrew, E. F. (1999). Spectral mixture analysis and geometric optical reflectance modelling of boreal forest biophysical structure. *Remote Sensing of Environment*, *67*, 297–388.

Rosema, A. W., Verhoef, W., Noorbergen, H., & Borgesius, J. J. (1992). A new forest light interaction model in support of forest monitoring. *Remote Sensing of Environment*, *42*, 23–41.

Rummel, R. J. (1970). *Applied factor analysis*. Evanston, IL: Northwestern University Press.

Sellers, P. (1985). Canopy reflectance, photosynthesis and transpiration. *International Journal of Remote Sensing*, *6*, 1335–1372.

Sellers, P. (1987). Canopy reflectance, photosynthesis and transpiration: II. The role of biophysics in the linearity of their interdependence. *Remote Sensing of Environment*, *21*, 143–183.

Soffer, R., Miller, J. R., Wanner, W., & Strahler, A. H. (1995). Winter forest BRF results: Comparisons between airborne data, laboratory simulations and geometrical–optical model data. *Proceedings of the 1995 IEEE International Geoscience and Remote Sensing Symposium, vol. 1* (pp. 800–805). Piscataway, NJ: IEEE (10–14 July, Firenze, Italy).

Valentine, F. A. (1964). *Convex sets*. New York: McGraw-Hill.

Vane, G., Green, R. O., Chrien, T. G., Enmark, H. T., Hansen, E. G., & Porter, W. M. (1993). The airborne visible/infrared imaging spectrometer (AVIRIS). *Remote Sensing of Environment*, *44*, 127–143.

Verhoef, W. (1984). Light scattering by leaf layers with application to canopy reflectance modelling: The SAIL model. *Remote Sensing of Environment*, *16*, 125–141.